FRIGID ZONE **MEDICINE**
Original Article • DOI: 10.1515/fzm-2024-0021

GDF11 restores the impaired function of EPCs-MA by promoting autophagy: GDF11 ameliorates endothelial progenitor cell aging by promoting autophagy

Donghua Liu[1*], Yang Zhang[2], Xin Liu[2], Qihe Huang[2], Xiaofang Zhang[2], Rui Yang[2], Yue Zhao[3], Penghui Li[2], Jiayi He[1], Kexiao Zhang[1], Zhenwei Pan[2,4,5], Huiwen Liu[1], Baofeng Yang[2,4,6*]

Abstract

Objective: Our study aimed to assess the effects of Growth and differentiation factor 11 (GDF11) on the function of endothelial progenitor cells in middle-age individuals (EPCs-MA) isolated from mouse bone marrow and to explore the mechanistic relationship between GDF11 and age-related ALP impairment. **Methods:** Bone marrow-derived EPCs were isolated, culture and GDF11 treatment. *In vivo*, the mice model of myocardial ischemia (MI) was induced by permanent ligation of the left anterior descending coronary artery (LAD) and mice were randomly divided into MI group and EPCs transplantation group (EPCs-Y, EPCs-MA, EPCs-MA/GDF11). The positive effect of GDF11 treatment of EPCs-MA on MI was verified by echocardiography and the average ratio of fibrotic area to left ventricular (LV) area. *In vitro*, the effect of GDF11 on ameliorating EPCs aging by promoting autophagy was confirmed by transwell assay, immunofluorescence staining, characterization of EPCs ultrastructure through transmission electron microscope (TEM), lysosome imaging and Western blot. **Result:** Our findings demonstrate that GDF11 enhances the migration capacity of EPCs-MA and improves recovery of impaired cardiac function after myocardial infarction (MI) in mice, with EPCs isolated from young mice (EPCs-Y) as controls. Moreover, GDF11 restored functional phenotypes of EPCs-MA to levels akin to EPCs-Y, promoting the expression of CD31, endogenous NO synthase, and the restoration of von Willebrand factor (vWF) and CDH5 expression patterns, as well as the formation of Weibel-Palade bodies—key organelles for storage and secretion in endothelial cells and EPCs. Furthermore, GDF11 significantly enhanced the autophagic clearance capability of EPCs-MA by promoting ALP. **Conclusions:** Our results suggest that GDF11 ameliorates cardiac function impairment by restoring the activities of EPCs from aging mice through enhanced ALP. These findings suggest that GDF11 may hold therapeutic potential for improving aging-related conditions associated with declined autophagy.

Keywords

GDF11; endothelial progenitor cells; autophagy lysosome pathway; aging

Received 22 February 2024, accepted 17 September 2024

[1]*Department of Histology and Embryology, Harbin Medical University, Harbin 150081, China*
[2]*Department of Pharmacology, Harbin Medical University (State-Province Key Laboratories of Biomedicine-Pharmaceutics of China, Key Laboratory of Cardiovascular Research, Ministry of Education), Harbin Medical University, Harbin 150081, China*
[3]*Department of Pharmacy at the Second Affiliated Hospital, Harbin, 150086, China*
[4]*Research Unit of Noninfectious Chronic Diseases in Frigid Zone, Chinese Academy of Medical Sciences, 2019RU070, Harbin 150081, China.*
[5]*NHC Key Laboratory of Cell Transplantation, The First Affiliated Hospital of Harbin Medical University, Harbin 150081, China*
[6]*Translational Medicine Research and Cooperation Center of Northern China, Heilongjiang Academy of Medical Sciences, Harbin 150081, China*

**Corresponding author Donghua Liu, E-mail: liudh@hrbmu.edu.cn; Baofeng Yang, E-mail: yangbf@ems.hrbmu.edu.cn*

1 Introduction

Growth and differentiation factor 11 (GDF11) is a circulating molecule associated with the aging processes of various tissues[1-6]. Recent studies show that GDF11 enhances the migration of endothelial progenitor cells (EPCs) isolated from adult peripheral blood *in vitro* and improves the angiogenic function of EPCs from diabetic rats *in vivo*[7-8]. Moreover, overexpression of GDF11 in the heart improves cardiac function and promotes the homing of EPCs, thereby facilitating angiogenesis in ischemic hearts of aged mice[9].

EPCs represent a heterogeneous population of cells in the bone marrow (BM), mobilized to peripheral circulation and recruited to ischemic tissues to promote adult neovascularization, contributing to tissue regeneration[10-11]. However, the functionality of EPCs declines progressively with aging[12]. A meta-analysis indicates that reduced levels of circulating cells with vasculoregenerative

properties, including EPCs, are associated with increased risk factor for adverse cardiovascular outcomes and mortality[13]. This suggests that early intervention of EPCs aging are essential for prevention of cardiovascular disease (CVD) highly varied impacted by ambient temperature in middle-aged individuals and GDF11 may counteract the age-dependent reduction of BM derived EPCs-MA. Aging is characterized by the progressive deterioration of cells and organs due to the accumulation of macromolecular and organelle damages, alongside a gradual decline in autophagic activity[14]. Macroautophagy (autophagy) plays a critical role in cellular degradation processes[15-17]. The continuous removal of damaged components and replacement with newly synthesized substances maintain cellular homeostasis and delay the aging process[18]. Several autophagy-inducing agents are currently under investigation in clinical trials for their potential as anti-aging therapies[19]. Given that lysosomal function is closely linked to aging, enhancing lysosomal activity to boost autophagy represents a promising strategy for developing anti-aging agents and treatments for aging-related diseases[20]. However, it is still unclear whether GDF11 can be used for anti-aging therapies as autophagy regulator in middle-aged individuals.

TGF-β signaling is recognized as an autophagy regulator that promotes autophagy activity during the development of Caenorhabditis elegans[21]. As a secreted factor of the TGF-β family of cytokines[22], GDF11 may help restore the age-dependent dysfunction of EPCs by increasing autophagic activity. Based on these findings, we hypothesize that GDF11 ameliorates the impairment of EPCs-MA by promoting the autophagy-lysosome pathway (ALP).

2 Materials and Methods

2.1 Animal care

Healthy male C57BL/6 mice aged 2 to 8 months were purchased from Beijing Vital River Laboratory Animal Technology Co., Ltd. The mice were housed under standard conditions (temperature: 21.1°C; humidity: 55%-60%) with free access to food and water for 2 to 4 weeks prior to experimental interventions. Use of animals was approved by the Ethic Committees of Harbin Medical University and conformed to the Guide for the Care and Use of Laboratory Animals published by the US National Institutes of Health (NIH Publication No. 85-23, revised 1996).

2.2 Isolation, culture and GDF11 treatment of BM-derived EPCs

BM cells were harvested by flushing the tibias and femurs of age-matched (8-10 weeks or 7-8 months) donor mice. BM-derived mononuclear cells (BM-MNCs) were isolated using density gradient centrifugation with Histopaque-1083 (Sigma-Aldrich). The cells were then plated onto culture dishes precoated with human fibronectin (Gene operation, YESEN, China), and maintained in EGM-2-MV BulletKit (CC-3202, Lonza Clonetics). After 4 days in culture, non-adherent cells were removed by washing with PBS, and the cells were incubated in fresh medium t from days 7 to 10[23]. For GDF11 treatment, EPCs were incubated with recombinant human GDF11 (PeproTech) at a final concentration of 80 ng/mL in EGM-2 BulletKit (CC-3162, Lonza Clonetics) from days 8 to 10, after which the cells were harvested for subsequent assays. EPCs derived from two-months-old (2M) and 7-8M-old mice were designated EPCs-Y and EPCs-MA, representing cells from young and middle-age mice, respectively. For morphological analysis, three cell colonies (each containing at least 58 cells) were counted per batch.

2.3 Animal model of myocardial ischemia

All animal procedures were approved by the Animal Care and Use Committee of the Harbin Medical University. Male C57BL/6 mice aged 8-10 week were anesthetized with a ketamine-xylazine mixture (100 mg/kg and 5 mg/kg, i.p.). A polyethylene tube was intubated orally for artificial respiration (UGO Bsile S.R.L. Biological Research Apparatus, Italy). A left thoracotomy was performed through the fourth intercostal space, and the pericardium was opened to expose the heart. The left anterior descending coronary artery (LAD) was ligated a silk thread (5/0 for rats or 7/0 for mice) to induce infarction of the left ventricular free wall. Cardiac infarction was confirmed by S-T segment elevation on ECG and cyanosis of the myocardium. After surgery, the mice had ad libitum access to food and water[24].

2.4 Transplantation of EPCs

One hour after the induction of myocardial ischemia (MI), mice with or without GDF11 treatment received intravenous injections of 1×10^6 late-outgrowth EPCs-MA resuspended in 200 μL of EBM-2 (n = 5). Mice that underwent MI without treatment served as the blank control. Mice were sacrificed 14 days post-MI[25].

2.5 Physiological assessment of LV function

Transthoracic echocardiography was performed 14 days after MI using a Vivid 7 GE medical ultrasound machine equipped with a 10-MHz phased-array transducer. Measurements included left ventricular systolic diameter (LVSd), left ventricular diastolic diameter (LVDd), interventricular septum diastolic thickness (IVSd), and interventricular septum systolic thickness (IVSs). Left ventricular ejection fraction (EF) and fractional shortening (FS) were calculated from the M-mode recording. After functional measurement, the mice were euthanized, and the hearts were dissected and fixed in 4% paraformaldehyde for histological assessment[24].

2.6 Histological assessment of transplanted animals

Following fixation, myocardium samples were sliced into three transverse sections from apex to base in a bread-loaf fashion. Paraffin-embedded peri-infarction specimens were analyzed to measure the average ratio of fibrotic area to LV area[25].

2.7 Characterization and immunofluorescence staining of EPCs

EPCs were grown on sterilized 24-mm glass slides. For characterization, cells were treated with 30 μg/mL 1,1'-dioctadecyl-3,3,3',3-tetramethyl-indocarbocyanine perchlorate-labeled acLDL (acLDL-DiI, 3mg/mL; Yiyuan Biotechnologies Inc., Guangzhou, China) at 37°C for 4 h. After 7 days in culture, EPCs were fixed in 1 mL of 2% paraformaldehyde (PFA) at room temperature (RT) for 1 h. Following a PBS wash, the cells were incubated with 10 μg/mL FITC-conjugated BS-1 lectin (2 mg/mL, Sigma-Aldrich) at 4°C for 2 h. After another PBS wash, DAPI nuclear staining was performed. For immunofluorescence staining, cells were fixed in 1 mL of 4% paraformaldehyde in PBS at 4°C for 3 h, washed twice with ice-cold PBS, and incubated in 10% goat serum/PBS/0.1%-Triton-X100 at RT for 1 h[26]. Cells were then incubated overnight at 4°C with primary antibodies against CDH5(BS-0878R, Bioss), CD31(BS-0195R, Bioss), eNOS (ENT3173, Elabscience), and Von Willebrand Factor (vWF) (BS-10048R, Bioss), followed by 1 h at RT. After washing three times with PBST (PBS with 0.05% TWEEN20), the cells were incubated with a secondary antibody (Anti-Rabbit Alexa Fluor® 594, ab150072) at RT for 1 hr. After three washes with PBST, the stained cells were mounted in mounting medium containing DAPI or Hoechst33342. Specimens were examined under a Zeiss fluorescence microscope equipped with an epifluorescence and Axiocam camera system, and analyzed using Axiovision software (Carl Zeiss, Oberkochen, Germany). Three fields were counted on each slide, with at least 58 cells were counted per field. Duplicate determinations were performed for each experimental condition.

2.8 Transwell assay

A modified Boyden chamber assay was performed using a 24 well-transwell plate with 8-μm pore size polycarbonate membranes (Corning Costar, Acton, MA). Cells were cultured for 10 days with EGM-2, trypsinized, and counted. A fraction of 8 × 104 cells in 100 μL non-FBS EBM-2 was seeded into the upper chamber, and 600 μL culture medium containing 1% FBS was added into the lower chamber[27]. EPCs were allowed to migrate in the tissue culture incubator at 37°C for 24 h. To quantify the number of migrated EPCs, the upper side of the membrane was washed with cold PBS, and remaining cells were removed with a cotton swab. Cells adhered to the lower surface of the membrane were stained with a 0.1% crystal violet solution[52]. The number of migrated cells in six randomly selected fields was counted under a light microscope (magnification, 200×; Olympus, Tokyo, Japan). Three fields were counted on each membrane in duplicate. Migration results are expressed as the mean value of total number of migrated cells per field.

2.9 Characterization of EPCs ultrastructure

The ultrastructure of BMEPCs was examined under a transmission electron microscope (TEM). EPCs were harvested after 10 days in culture, treated with 0.03% trypsin without EDTA, resuspended in 1 mL EBM without FBS in 1.5 mL Eppendorf tube, and centrifuged at 4°C for 10 min (2000 rpm). Cells were fixed immediately in 2.5% cold glutaraldehyde in PBS (pH 7.2) at 4°C for 2 h. After rinsing with PBS, cells were post-fixed in 1% osmium tetroxide at 4°C for 1 hr, followed by dehydration in gradient acetone at 4°C and embedded in Epon812. The resultant blocks were sliced into ultra-thin sections (70 nm) using an ultra-thin slicer and double-stained with uranyl acetate and lead citrate. Specimens were examined under a transmission electron microscope (H-7650 TEM; Hitachi, Tokyo, Japan).

2.10 Western blot analysis

EPCs were harvested with trypsin-EDTA and centrifuged at 500 × g for 5 min. The resulting cell pellets were suspended in PBS and then transferred to a 1.5-mL microcentrifuge tube, followed by an additional centrifugation at 500 × g for 3 min. The cell pellets were then lysed on ice in RIPA buffer containing protease and phosphatase inhibitors. Protein concentration was determined using the bicinchoninic acid (BCA) protein assay. For Western blotting, 80 μg of total protein was separated using 10% or 12.5% sodium dodecyl sulfate-polyacrylamide gel electrophoresis (SDS-PAGE) and transferred onto nitrocellulose membranes (Merck Millipore, R7BA46025 or Pall Corporation, 66485). The membranes were blocked in PBS containing 5% nonfat milk at room temperature (RT) for 70 min, or a in Western Quick Block Kit (L00276, GenScript) at RT for 20 min. The blots were then incubated overnight at 4°C with primary antibodies diluted in PBS[28]. The primary antibodies used included p62 (BS2951R, Bioss or 380612, ZenBio), LC3B (AL221, Beyotime, Biotechnology), and GAPDH (AC002 or AC033, ABclonal), with GAPDH serving as an internal control for sample input. After washing the membranes with PBST, d they were incubated for 1 hour at RT with a secondary antibody (Alexa Fluor, or LICOR). Finally, Western blot images were captured using an imaging system (Odyssey, LICOR, USA) and quantified by measuring the intensities using Odyssey v1.2 software. Results were expressed as fold-changes after normalization to the control values.

2.11 Lysosome imaging

To assess lysosomal acidification, EPCs were incubated in endothelial growth medium (EGM) containing 75 nmol/L LysoTrackerRed (Red DND-99, L7528 Invitrogen) for 2 h. Following incubation, cells were imaged immediately using a Zeiss fluorescence microscope equipped with an epifluorescence system, an Axiovision camera, and Axiovision software (Carl Zeiss, Oberkochen, Germany).

2.12 Statistical analysis

Data analyses were performed using GraphPad Prism9. Error bars in all graphs present standard deviations. Comparisons between two groups were performed using the two-tailed Student's *t*-test. *P* values of less than 0.05 were considered statistically significant difference.

3 Results

3.1 GDF11 changes the ratio of different subpopulations of EPCs-MA

In the present study, murine BM mononuclear cells (BMMNCs) were isolate from young- (8-10 weeks old) and middle-aged (7-8 months old) mice[29]. EPCs, characterized as cells forming cobblestone colonies on days 9-14 in culture, are reported to possess the highest angiogenic potential[30]. Therefore, EPCs at day 10 were used for the experiments, with GDF11 treatment applied to the cells on day 8 for 48 hours prior to assay collection.

Under normal culture conditions, the attached cells exhibited typical characteristics of EPCs at D10: clusters surrounded by spindle-like cells were formed on FN-coated tissue culture plates. These cells exhibited four morphologic types: drop-like cells (round shape cells) (arrowhead), spindle-like cells (early EPC)(arrow), cobblestone-like cells (late EPC) (black star)[31], and flatten round cells (red star) (Fig. 1A). Statistical analysis indicated no significant difference in the proportion of spindle-like cells between the two groups either (Fig. 1B). However, the percentage of spindle-like cells was significantly increased in EPCs-MA pretreated with GDF11, indicating that GDF11 may act through changing the proportion of cell subpopulations of EPCs (Fig. 1B). Under standard culture conditions, the attached cells demonstrated typical EPC characteristics at day 10: clusters of cells surrounded by spindle-shaped cells formed on fibronectin-coated tissue culture plates. Morphologically, these cells exhibited four distinct types: drop-like cells (round-shaped) (arrowhead), spindle-like cells (early EPC) (arrow), cobblestone-like cells (late EPC) (black star), and flattened round cells (red star) (Fig. 1A). Statistical analysis revealed no significant difference in the proportion of spindle-like cells between the two groups (Fig. 1B). However, a significant increase in the percentage of spindle-like cells was observed in EPCs-MA pretreated with GDF11, suggesting that GDF11 may modulate the subpopulation ratios of EPCs (Fig. 1B).

To differentiate EPCs-MA from EPCs-Y, uptake of Dil-Ac-LDL and binding of lectin UEA-1 (Lectin1) were assessed. As illustrated in Fig. 1C, both EPCs-MA and EPCs-Y were identified as Dil-Ac-LDL+Lectin1+ cells, indicating their ability to uptake Dil-Ac-LDL from the culture medium and bind to lectin UEA-1 (Lectin1). GDF11 pretreatment did not alter this property (Fig. 1C).

We assessed the expression of classical EPC surface markers, specifically VE-cadherin (CDH5 or CD144), found in the initial drop-like EPCs (round-shaped cells), and CD31, which was expressed in EPCs g that acquire endothelial properties at later stages[32]. Our findings revealed that 100% of EPCs-Y and EPCs-MA expressed CDH5, albeit at varying levels: high expression in larger drop-like cells, medium expression in spindle-like (early EPCs), and low expression in cobblestone-like cells (late EPCs). This suggests that CDH5 expression may diminish with EPCs maturation. Notably, more than half of the EPCs-Y expressed CDH5 at low levels in EPCs-MA was reduced, with GDF11 pretreatment restoring levels to approximate those seen in EPCs-Y (Fig. 2A and 2B). CD31 was expressed in the majority of EPCs-Y and EPCs-MA, indicating the acquisition of endothelial cell characteristics with EPCs maturation. However, the percentage of CD31-positive cells in EPCs-MA significantly declined compared to EPCs-Y. Following GDF11 pretreatment, although the proportion of CD31-expressing cells increased, it remained significantly lower than that observed in EPCs-Y (Fig. 2A and 2C).

3.2 GDF11 improves the function of EPCs-MA *in vitro* and *in vivo*

We examined the effects of GDF11 on EPCs-MA both *in vitro* and *in vivo*, with the experimental procedures outlined in Fig. 3A. For the functional assays, EPCs on day 10 were used for migration assays *in vitro* (migration assay) and for EPC transplantation therapy in MI mice. The migration assay results demonstrated a significant decrease in the migrating capability of EPCs-MA compared with EPCs-Y. Notably, the impaired migration was partially restored in EPCs-MA pretreated with GDF11. The concentration of GFF11 used in these experiments was determined based on its effect on EPC migration (Fig. 3B).

To assess the impact of EPCs on cardiac function, echocardiography was performed 2 weeks post-transplantation in MI mice. As depicted in Fig. 3C, transplantation of EPCs-Y markedly improved the MI-induced decreases in EF and FS, while EPCs-MA

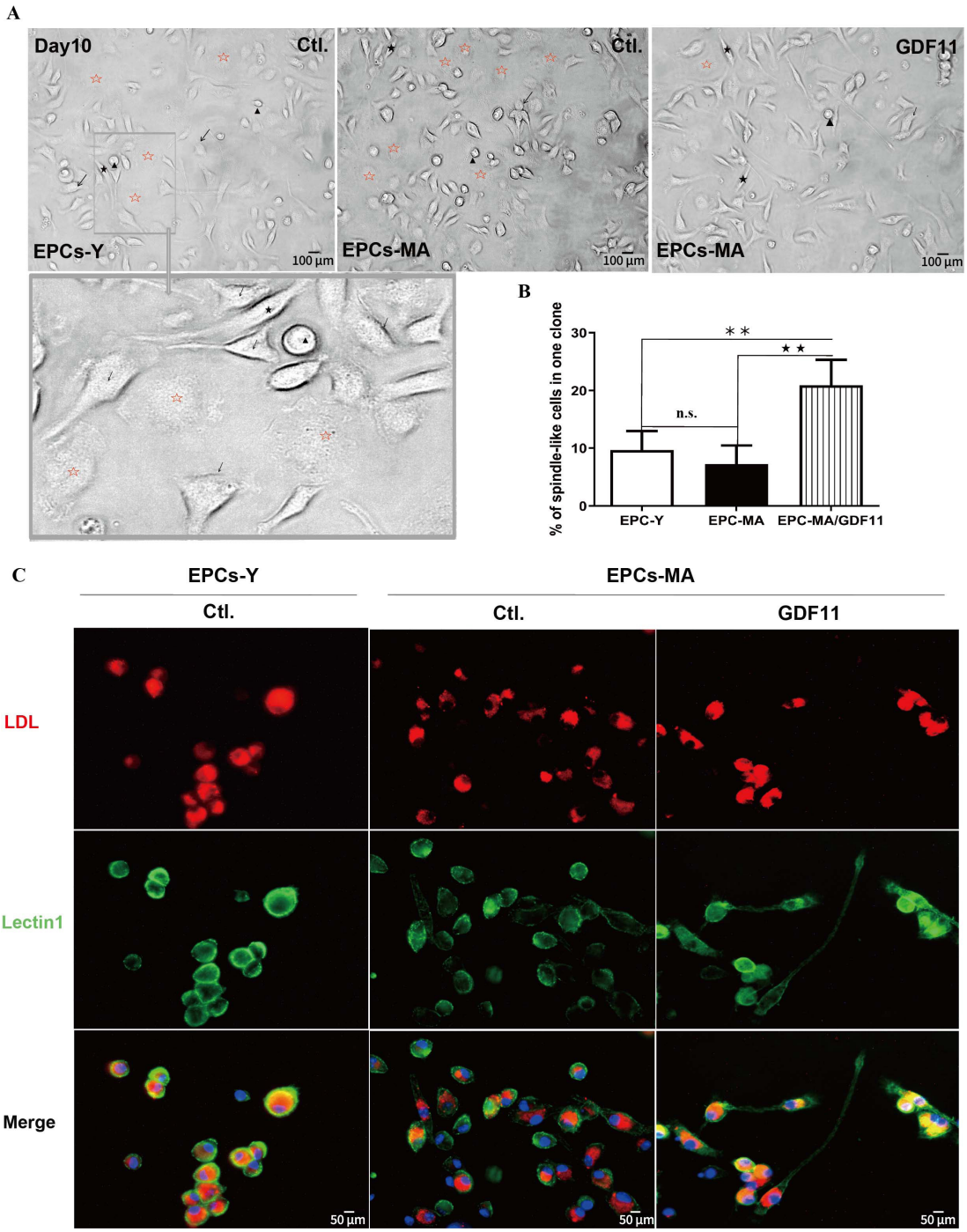

Fig. 1 GDF11 changes the ratio of different subpopulations of EPCs-MA based on morphological features

(A) Light microscopic photographs showing mononuclear cells (MNCs) at day 10 in the culture with clusters of cells surrounded by spindle-like cells. Four morphologic subtypes were identified: cobblestone-like cells, spindle-like cells, drop like cells, and flatten round cells, which are marked with arrows, dark stars, arrowheads, and hollowed red stars, respectively. (B) Bar chart showing the percentage of spindle-like cells relative to other subtypes of EPCs. Statistical data on the ratio of spindle-like cell subpopulation are expressed as the mean values of percent spindle-like cells over total number of EPCs per EPCs clones (n = 2 batches in each group). (C) Representative fluorescence images with red staining depicting cells engaging in active Dil-Ac-LDL uptake from the culture medium and green staining for EPCs with lectin UEA-1 (lectin1) binding. The spindle-like cell is marked with black stars; Scale bar: (A) 100 μm and (C) 50 μm; $^{**}P < 0.01$, $^{\star\star}P < 0.01$.

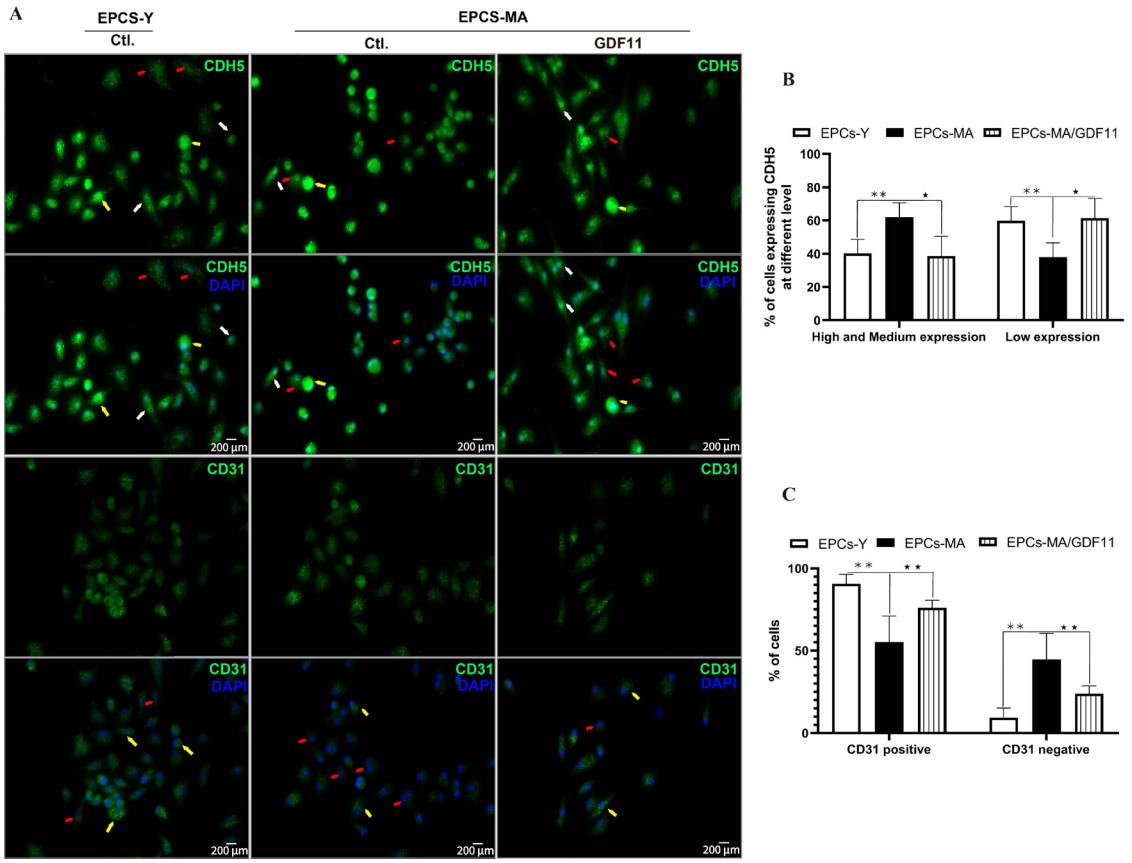

Fig. 2 Effects of GDF11 on EPCs-MA maturation

Immunofluorescence staining showing the expression and distribution of CDH5 (green) and CD31 (green) primarily in the plasma membrane. (A) CDH5 expressed in EPCs at varying levels and can be classified into low (red arrow), medium (yellow arrow), and high (white arrow) level based on the fluorescence intensity. The majority of EPCs expressed CD31 (yellow arrow), CD31 was negative in few cells (red arrows). (B) Bar chart showing percent cells expressing CDH5 at low, medium, and high levels. (C) Bar chart showing the percentage of CD31 positive and negative cells. Scale bar: 100 μm; $^{**}P < 0.01$, $^{\star}P < 0.05$, $^{\star\star}P < 0.01$.

produced only modest effects. In contrast, EPCs-MA pretreated with GDF11 resulted in enormous increases in both EF and FS, surpassing the beneficial effects observed with EPCs-Y.

To evaluate the effect of GDF11 on the structural impairments in MI hearts, histological examinations were conducted using Masson's trichrome staining. The results revealed significant collagen deposition, indicative of fibrosis in the infarct region of the mouse hearts. Transplantation of EPCs-Y markedly reduced cardiac fibrosis, whereas EPCs-MA elicited only a moderate beneficial effect. Notably, GDF11-pretrated EPCs-MA yielded enhanced anti-fibrotic capacity, as evidenced by the robust mitigation in the area of collagen deposition relative to non-GDF11-treated EPCs-MA (Fig. 3D). More strikingly, the infarct size was significantly diminished in mice transplanted with GDF11-pretreated EPCs-MA compared to those receiving non-treated EPCs-MA (Fig. 3E).

3.3 GDF11 restores the lost functional phenotypes of EPCs-MA

LOCs express endothelial markers, such as endothelial nitric oxide synthase (eNOS) and vWF[33], whose inhibition is associated with functional impairment of EPCs[34]. In our model, EPCs-MA exhibited significantly lower levels of eNOS (Fig. 4A and 4B) compared to EPCs-Y. Surprisingly but expectedly, GDF11 pretreatment remarkably boosted up eNOS expression in EPCs-MA. In terms of vWF expression, approximately 98.4% of EPCs-Y exhibited varying levels of vWF, with 78.7% at medium levels, and 14.8% and 4.9% at high and low levels, respectively. In contrast, only 73.1% of EPCs-MA expressed vWF, showing a decrease of 3.2% and 44.6% in high and medium expressers, respectively, and a 26.6% increase in low expressers. Following GDF11 treatment, the percentage of vWF-expressing EPCs-MA increased to 94.8%, with medium-level expressers increasing to 79.5%, aligning closely with the levels observed in EPCs-Y.

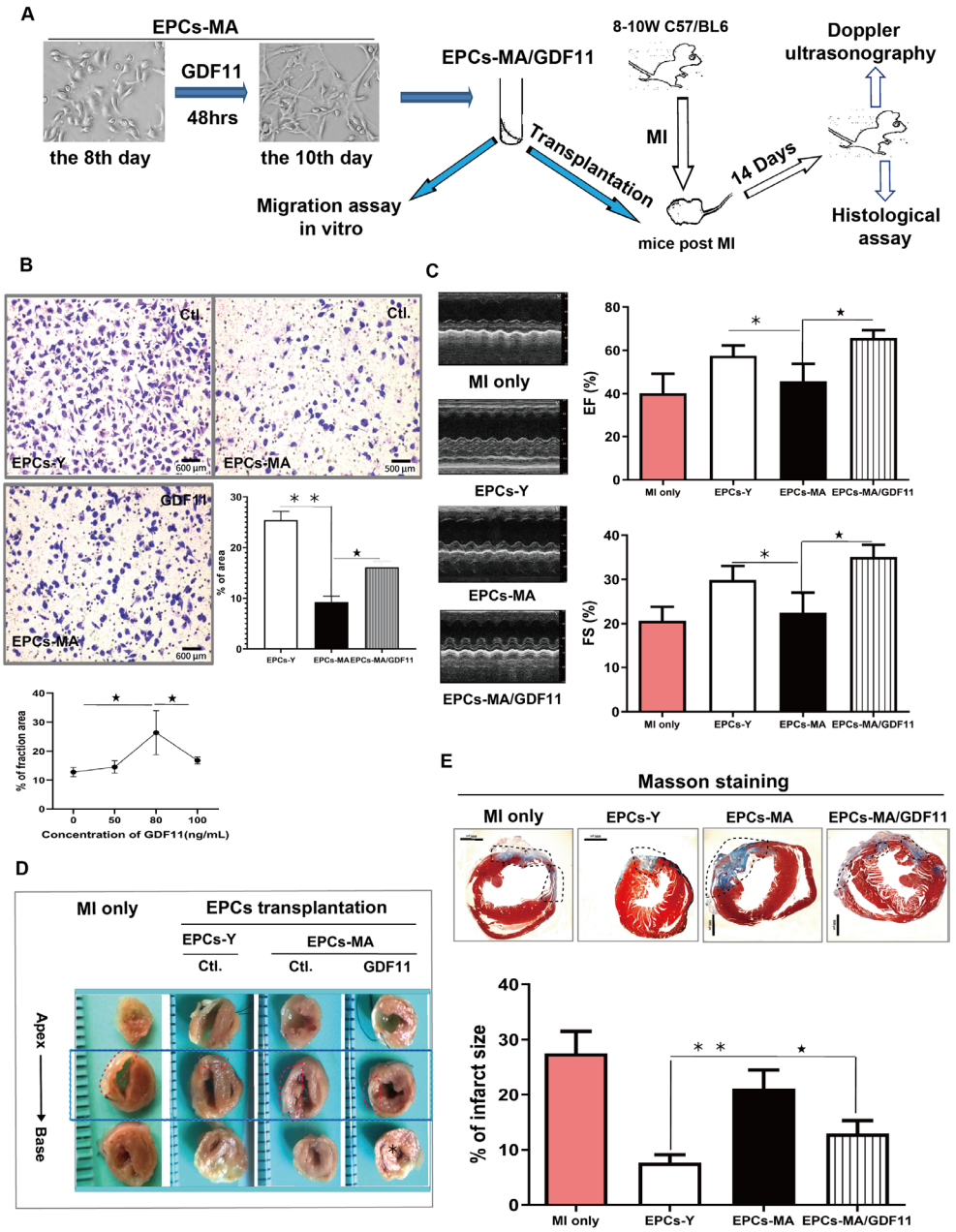

Fig. 3 Effects of GDF11 on EPCs-MA migration *in vitro* and *in vivo*

(A) The experiment procedures for migration assays of EPCs: Prior to EPCs collection, the cells at day 8 in culture were treated with GDF11 for 48 h. The EPCs at day 10 were used for migration assays *in vitro* and *in vivo*. For migration assays *in vivo*, 8-10-weeks-old mice were subject to MI surgery and injection of EPCs *via* tail vein one-hour post-MI. After 14 days, Doppler ultrasonography and histological assays were performed to evaluate cardiac function and measure the infarct size. Statistical data were obtained from 3 independent experiments (n = 3-4 per group). (B) The effect of GDF11 on the migration of EPCs-MA: Migrated cells were visualized after crystal violet staining in blue color. The bar chart present the percentages of migrated cell areas (n = 3 batches per group). Scale bar: 500 μm. (C) Echocardiographic assays depicting the changes of ejection fractions (EF) and fractional shortening (FS) of left ventricle (LV). Cardiac functional parameters of the MI mice and EPCs-Y-transplanted mice were used as negative and positive controls, respectively. n = 5-7/group. (D and E) The hearts were diseected into 3-4 parts from apex to base (D), and peri-infarct tissues (squared) were sectioned and stained with Masson trichrome for assessing infarct size. Fibrotic tissues were stained blue, and the viable tissues were stained red. Collagen (CoL) deposition was quantified with an automated image analyzer, and the data are expressed as percentage of tissue areas. The bar graphs show infarcts size in different groups. Scale bar sizes in Masson section: 2000 μm (E); $^{*}P < 0.05$, $^{**}P < 0.01$, $^{\star}P < 0.05$.

Notably, the proportion of EPCs-MA expressing low levels of vWF further decreased to 12.4%, and no additional increase in high-level vWF expressers was observed (Fig. 4C and 4D).

vWF is implicated in both angiogenesis[35] and the formation of the Weibel-Palade bodies (WPBs) which are rod-shaped organelles found in the cytoplasm of endothelial cells[36] and EPCs[37]. Our analysis revealed a dramatic reduction in the number of WPBs in EPCs-MA compared to EPCs-Y (Fig. 4E and 4F). Notably, GDF11 pretreatment led to a significant increase in the number of WPBs with distinct shapes in the trans-Golgi network (TGN) of EPCs-MA, especially near the Golgi complex, mirroring the ultrastructural characteristics of EPCs-Y (Fig. 4E). The literature indicates that spindle-like cells contain abundant WPBs, whereas cobblestone-like cells possess fewer WPBs[37]. Our findings align with these observations; under light microscopy, GDF11-pretreated EPCs-MA exhibited fewer flattened round cells and a higher number of spindle-like cells (Fig. 1B). Given that WPBs are lysosome-related organelles sharing some compositional and physiological features with lysosomes[38], we aimed to determine whether GDF11 influences autophagic clearance in lysosomes.

3.4 GDF11 enhances the autophagic clearance capability of EPCs-MA

Aging is associated with a decline in autophagic flux, and pharmacological interventions that stimulate autophagy have been shown to promote longevity[7]. Moreover, autophagy plays an important role in improving the efficiency of EPC transplantation[39]. Therefore, we evaluated the effects of GDF11 on autophagic flux by assessing the expression of key autophagic proteins and the accumulation of autophagic vacuoles.

We first examined the conversion of LC3-I to LC3-II, an essential step in autophagosome formation[40]. As shown in Fig. 5A and 5B, the ratio of LC3-I to LC3-II was substantially higher in EPCs-MA than in EPCs-Y. However, this ratio was normalized in EPCs-MA pretreated with GDF11, indicating that GDF11 stimulates autophagy.

p62, which is selectively incorporated into autophagosomes through direct binding to LC3, is efficiently degraded by autophagy. Therefore, the total cellular expression level of p62 is inversely correlated with autophagic activity[41-42] with reduced expression of p62, indicating the activation of autophagy[43]. In our study, the total protein level of p62 in EPCs-MA was significantly elevated compared to EPCs-Y, but this difference was largely eliminated in GDF11-pretreated EPCs-MA (Fig. 5A and 5B), further supporting the notion that GDF11 favors autophagy.

Autophagy is a catabolic process that depends on the cooperation between autophagosomes and lysosomes[44]. Notably, lysosomes undergo significant alterations with aging[45]. Dysfunction in lysosomes can hinder autophagy, leading to decreased clearance of cellular debris and increased cellular senescence[46]. We observed a substantial accumulation of autophagic vacuoles in EPCs-MA, which was effectively mitigated after GDF11 pretreatment (Fig. 5C and 5D).

As illustrated in Fig. 5E, red fluorescence was markedly weaker in EPCs-MA than in EPCs-Y, suggesting that the pH within the lysosomal lumen was insufficiently acidic to support hydrolytic activity during autophagy. However, GDF11 pretreatment restored lysosomal acidity in EPCs-MA to levels comparable to those observed in EPCs-Y (Fig. 5F).

4 Discussion

In summary, this study demonstrates that EPCs derived from middle-aged (EPCs-MA) mice exhibit age-related phenotypic characteristics, including impaired migratory capacity, reduced expression of CD31 and eNOS, altered expression patterns of CDH5 and vWF, and impeded formation of WPBs (the organelles which store vWF), which collectively lead to a diminished ability to maintain cardiac function in post-MI mice. Notably, GDF11 pretreatment restored these impairments to levels comparable to those observed in EPCs-Y. Furthermore, GDF11 significantly enhanced the autophagic clearance capability of EPCs-MA, evidenced by lower p62 accumulation, a normalized LC3-I to LC3-II ratio, and reduced accumulation of autophagic vacuoles. This enhancement is associated with improved ALP function, indicated by enhanced lysosomal acidification. Consequently, GDF11 may serve as a novel therapeutic agent for anti-aging interventions and the treatment of aging-related diseases. Moreover, it is noteworthy that cold exposure has been shown to suppress eNOS expression and is linked to autophagy[48]. This raises the possibility that GDF11 could enhance EPC resistance to cold stress, an area we aim to explore in future studies.

EPCs play a pivotal role in promoting adult neovascularization and tissue regeneration in ischemic conditions[10-11]. However, starting in middle age, both the levels of circulating EPCs and their vascular regenerative capacity progressively decline due to multiple factors, including aging, smoking, and environmental stressors[13,49-51]. Our findings indicate that EPCs-MA exhibit compromised migratory and tissue repair capacities, reflected in their diminished ability to restore cardiac function and reduce infarct size in MI mice. At the molecular level, the reduced protein levels of CD31 and eNOS, along with the abnormal expression patterns of CDH5 and vWF, suggest impaired maturation of EPCs-MA. This maturation deficit may partially explain the observed

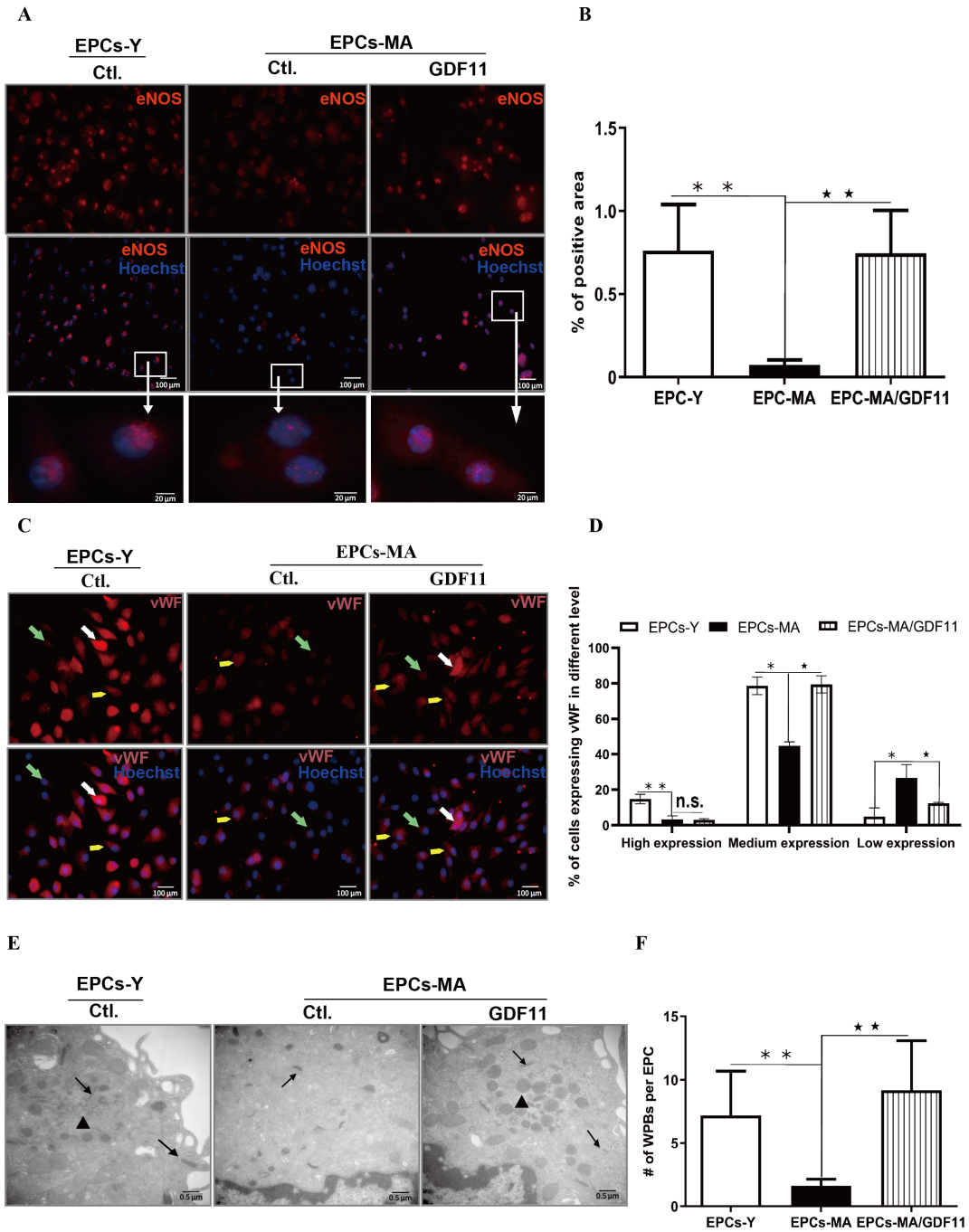

Fig. 4 GDF11 restores the lost functional phenotypes of EPCs-MA

(A and C) Typical examples of immunofluorescence staining images depicting the expression and subcellular distribution of eNOS (red) and vWF (red). eNOS was primarily expressed in the nuclear. In most of EPCs-MA, vWF exhibited a diffuse cytoplasmic signal. vWF was expressed in EPCs at different levels, allowing for classifications into low, medium, and high levels based on the fluorescence intensities. The majority of EPCs expressed vWF at a medium level (yellow arrow), and only small numbers of cells expressed vWF at high (white arrow) and low levels (green arrow), respectively. (B and D) Bar chart showing the percentage of positive area of eNOS expression and cells expressing vWF at low, medium, and high levels, respectively. (E) Photographs captured with TEM showing EPCs with elongated WPBs (arrows) and trans-Golgi networks (TGN) containing enlarged parts where WPBs are formed (arrows heads). (F) Bar chart presenting the mean numbers of WPCs per EPCs, a pile of TNG was recorded as 1 WPB; Scale bar: (A and C) 50 μm; E, 0.5 μm; $^{*}P < 0.05$, $^{**}P < 0.01$, $^{\star}P < 0.05$, $^{\star\star}P < 0.01$.

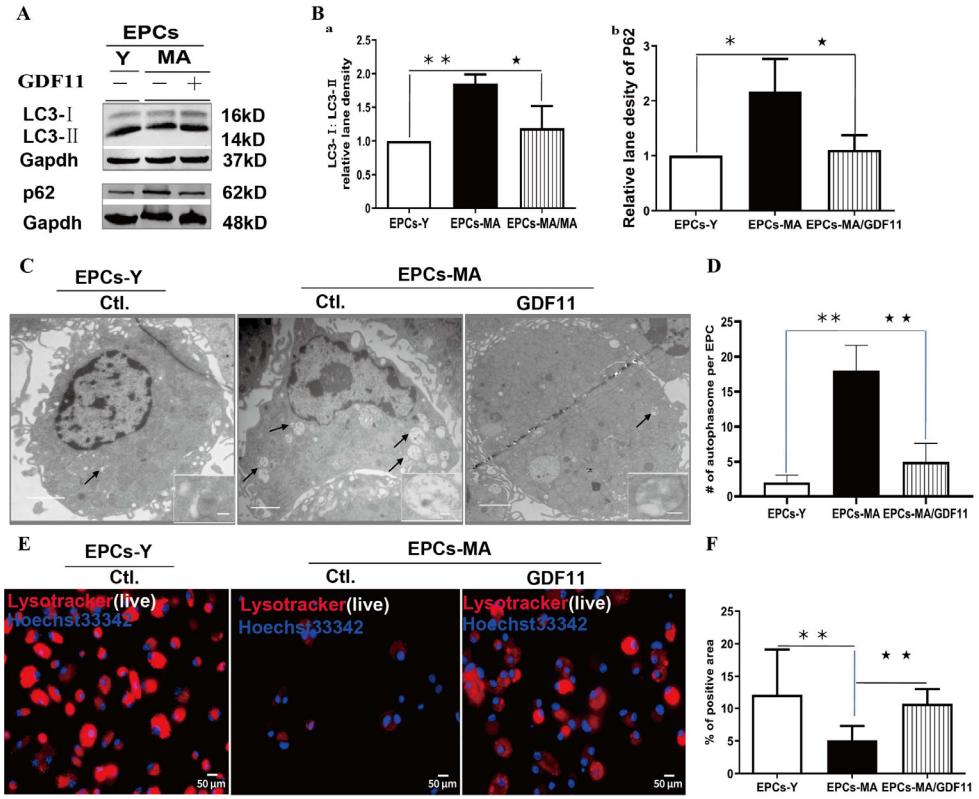

Fig. 5 GDF11 enhances autophagic clearance capability of EPCs-MA

(A) The effects of GDF11 on the conversion of endogenous LC3-I to LC3-II and p62 accumulation, as evidenced by by Western blot analysis. (B) Bar chart summarizing the ratio of LC3-I/LC3-II and relative protein levels of p62. GAPDH served as an internal control. (C) Autophagic vacuoles were counted under an electron microscope at 10,000× magnification. All autophagic vacuoles present in each photograph of EPC were counted. Scale bar: 1 μm and 200 nm. (D) Bar chart showing the number of autophagic vacuoles in each EPCs ($n = 3$). (E) Representative images of LysoTracker Red staining depicting the effects of GDF11 on the lysosomal acidification in EPCs. (F) Bar chart summarizing the percentage of positive areas (accumulated acidic organelles) in EPCs. $^{*}P < 0.05$, $^{**}P < 0.01$.

impairments in migratory function and the decreased numbers of circulating EPCs in middle age. The increased proportion of cells expressing low levels of vWF correlates with decreased WPB formation, indicating adverse ultrastructural changes. Research has shown that the spindle-like cells in EPCs are associated with WPB abundance[42], and the enhanced formation of WPBs in GDF11-pretreated EPCs-MA aligns with an increased ratio of spindle-like cells. Given that WPBs are lysosome-related organelles, the reduced WPB formation in EPCs-MA suggests lysosome dysfunction. Autophagy, a degradation process, relies on the interplay between autophagosomes and lysosomes[45]. Impaired ALP can compromise autophagy, leading to reduced autophagic clearance and autophagosome accumulation, which in turn promotes cellular senescence[46].

The total level of p62 is inversely correlated with autophagic activity[40-41], and increased p62 accumulation serves as a marker of disrupted autophagic flux[52]. Our findings confirm that EPCs-MA exhibit increased p62 levels and a higher LC3-I to LC3-II ratio, indicating autophagic flux perturbation. Additionally, we observed substantial accumulation of autophagic vacuoles in EPCs-MA, alongside insufficient lysosomal acidification necessary for effective hydrolytic activity during autophagy. Agents that induce autophagy and enhance lysosomal function offer promising avenues for intervention in aging and aging-related diseases[19-20].

The present study represents the first to unravel the facilitating effects of GDF11 on the conversion of LC3-I to LC3-II, the acidification of lysosomes, and the activation of ALP in EPCs-MA. Therefore, the enhanced autophagic clearance may contribute to the anti-aging property of GDF11.

In conclusion, our findings highlight the early cellular events associated with the aging process of EPCs and establish a mechanistic link between GDF11 and the impaired function of EPCs through modulation of ALP. Further studies are warranted to explore the potential of GDF11 as a novel therapeutic agent for aging and aging related diseases.

Acknowledgement

Not Applicable.

Author contributions

Liu D H: Experimental studies, Validation, Formal analysis, Writing-Original Draft, Funding, Statistical analysis; Zhang Y: Supervision, Funding; Liu X: Literature search, Experimental studies; data acquisition, Formal analysis, Validation; Huang Q H: Experimental studies; Zhang X F: Experimental studies; Yang R: Experimental studies; Zhao Y: Experimental studies; Li P H: Experimental studies; He J Y: Experimental studies; Zhang K X: Experimental studies; Pan Z W: Conceptualization, Resources, Supervision, Project administration, Funding, Experimental studies; Liu H W: Writing-Review and Editing, Supervision; Yang B F: Project administration, Funding, Conceptualization, Supervision, Resources, Writing-Review and Editing

Source of funding

Creative Research Groups of the National Natural Science Foundation of China (81421063); China Postdoctoral Science Foundation (2016M591556); Natural Science Foundation of Heilongjiang Province of China (H2016008); Postdoctoral Science Foundation of Heilongjiang Province of China (LBH-Z15146); Research Project of the Health and Family Planning Commission of Heilongjiang Province (2016-166).

Ethical approval

Healthy male C57BL/6 mice aged 2 to 8 months were used for animal studies (Animal Experimental Ethical Inspection Protocol Np. HMUIRB3021619). Use of animals was approved by Ethic Committees of Harbin Medical University and confirmed to the Guide for Care and Use of Laboratory Animals published by the US National Institutes of Health (NIH Publication No.85-23, revised 1996).

Informed consent

Not Applicable.

Conflict of interest

Yang B F is the editor-in-chief of Frigid Zone Medicine. This ariticle was subject to journal's standard procedures, while peer review handled independently of this Membr and his research groups.

Data availability statement

All data are available from the corresponding authors upon reasonable request.

References

[1] Loffredo F S, Steinhauser M L, Jay S M, *et al.* Growth differentiation factor 11 is a circulating factor that reverses age-related cardiac hypertrophy. Cell, 2013; 153: 828-839.
[2] Rochette L, Zeller M, Cottin Y, *et al.* Growth and differentiation factor 11 (GDF11): Functions in the regulation of erythropoiesis and cardiac regeneration. Pharmacol The, 2015; 156: 26-33.
[3] Katsimpardi L, Litterman N K, Schein P A, *et al.* Vascular and neurogenic rejuvenation of the aging mouse brain by young systemic factors. Science, 2014; 344: 630-634.
[4] Castellano J M, Kirby E D, Wyss-Coray T. Blood-borne revitalization of the aged brain. JAMA Neurol, 2015; 72: 1191-1194.
[5] Mendelsohn A R, Larrick J W. Systemic factors mediate reversible age-associated brain dysfunction. Rejuvenation Res, 2014; 17 : 525-528.
[6] Olson K A, Beatty A L, Heidecker B, *et al.* Association of growth differentiation factor 11/8, putative anti-ageing factor, with cardiovascular outcomes and overall mortality in humans: analysis of the Heart and Soul and HUNT3 cohorts. Eur Heart J, 2015; 36: 3426-3434.
[7] Finkenzeller G, Stark G B, Strassburg S. Growth differentiation factor 11 supports migration and sprouting of endothelial progenitor cells. J Surg Res, 2015; 198: 50-56.
[8] Zhang J, Li Y, Li H, *et al.* GDF11 improves angiogenic function of EPCs in diabetic limb ischemia. Diabetes, 2018; 67: 2084-2095.
[9] Guo Q D, Shao Z B, Wu J, *et al.* Targeted myocardial delivery of GDF11 gene rejuvenates the aged mouse heart and enhances myocardial regeneration after ischemia-reperfusion injury. Basic Res Cardiol, 2017; 112: 7.
[10] Hill J M, Zalos G, Halcox J P, *et al.* Circulating endothelial progenitor cells, vascular function, and cardiovascular risk. N Engl J Med, 2003; 348: 593-600.
[11] Asahara T, Murohara T, Sullivan A, *et al.* Isolation of putative progenitor endothelial cells for angiogenesis. Science, 1997; 275: 964-967.
[12] Thum T, Hoeber S, Froese S, *et al.* Age-dependent impairment of endothelial progenitor cells is corrected by growth-hormone-mediated increase of insulin-like growth-factor-1. Circ Res, 2007; 100: 434-443.
[13] Rigato M, Avogaro A, Fadini G P. Levels of circulating progenitor cells, cardiovascular outcomes and death: a meta-analysis of prospective observational studies. Circ Res, 2016; 118: 1930-1939.
[14] Mizushima N, Levine B, Cuervo A M, *et al.* Autophagy fights disease

through cellular self-digestion. Nature, 2008; 451: 1069-1075.
[15] Nakamura S, Yoshimori T. New insights into autophagosome-lysosome fusion. J Cell Sci, 2017; 130: 1209-1216.
[16] Bejarano E, Yuste A, Patel B, *et al.* Connexins modulate autophagosome biogenesis. Nat Cell Biol, 2014; 16: 401-414.
[17] Sinha M, Jang Y C, Oh J, *et al.* Restoring systemic GDF11 levels reverses age-related dysfunction in mouse skeletal muscle. Science, 2014; 344: 649-652.
[18] Rajawat Y S, Hilioti Z, Bossis I. Aging: central role for autophagy and the lysosomal degradative system. Ageing Res Rev, 2009; 8: 199-213.
[19] Levine B, Kroemer G. Autophagy in aging, disease and death: the true identity of a cell death impostor. Cell Death Differ, 2009; 16: 1-2.
[20] Carmona-Gutierrez D, Hughes A L, Madeo F, *et al.* The crucial impact of lysosomes in aging and longevity. Ageing Res Rev, 2016; 32: 2-12.
[21] Guo B, Huang X, Zhang P, *et al.* Genome-wide screen identifies signaling pathways that regulate autophagy during Caenorhabditis elegans development. EMBO Rep, 2014; 15: 705-713.
[22] Egerman M A, Glass D J. The role of GDF11 in aging and skeletal muscle, cardiac and bone homeostasis. Crit Rev Biochem Mol Biol, 2019; 54: 174-183.
[23] Kalka C, Masuda H, Takahashi T, *et al.* Transplantation of ex vivo expanded endothelial progenitor cells for therapeutic neovascularization. Proc Natl Acad Sci U S A, 2000; 97: 3422-3427.
[24] Pan Z, Sun X, Shan H, *et al.* MicroRNA-101 inhibited postinfarct cardiac fibrosis and improved left ventricular compliance *via* the FBJ osteosarcoma oncogene/transforming growth factor-β1 pathway. Circulation, 2012; 126: 840-850.
[25] Kawamoto A, Gwon H C, Iwaguro H, *et al.* Therapeutic potential of ex vivo expanded endothelial progenitor cells for myocardial ischemia. Circulation, 2001; 103: 634-637.
[26] Masuda H, Iwasaki H, Kawamoto A, *et al.* Development of serum-free quality and quantity control culture of colony-forming endothelial progenitor cell for vasculogenesis. Stem Cells Transl Med, 2012; 1: 160-171.
[27] Tang Y, Vater C, Jacobi A, *et al.* Salidroside exerts angiogenic and cytoprotective effects on human bone marrow-derived endothelial progenitor cells *via* Akt/mTOR/p70S6K and MAPK signalling pathways. Br J Pharmacol, 2014; 171: 2440-2456.
[28] Yu M, Chen Y, Li X, *et al.* YAP1 contributes to NSCLC invasion and migration by promoting Slug transcription *via* the transcription co-factor TEAD. Cell Death Dis, 2018; 9: 464.
[29] Reines B, Cheng L I, Matzinger P. Unexpected regeneration in middle-aged mice. Rejuvenation Res, 2009; 12: 45-52.
[30] Ikutomi M, Sahara M, Nakajima T, *et al.* Diverse contribution of bone marrow-derived late-outgrowth endothelial progenitor cells to vascular repair under pulmonary arterial hypertension and arterial neointimal formation. J Mol Cell Cardiol, 2015; 86: 121-135.
[31] Wang X, Wang R, Jiang L, *et al.* Endothelial repair by stem and progenitor cells. J Mol Cell Cardiol, 2022; 163: 133-146.
[32] Salybekov A A, Kobayashi S, Asahara T. Characterization of endothelial progenitor cell: past, present, and future. Int J Mol Sci, 2022; 23(14): 7697.
[33] Altabas V, Altabas K, Kirigin L. Endothelial progenitor cells (EPCs) in ageing and age-related diseases: how currently available treatment modalities affect EPC biology, atherosclerosis, and cardiovascular outcomes. Mech Ageing Dev, 2016; 159: 49-62.
[34] Michaud S E, Dussault S, Haddad P, *et al.* Circulating endothelial progenitor cells from healthy smokers exhibit impaired functional activities. Atherosclerosis, 2006; 187: 423-432.
[35] Caiado F, Dias S. Endothelial progenitor cells and integrins: adhesive needs. Fibrogenesis Tissue Repair, 2012; 5: 4.
[36] Zenner H L, Collinson L M, Michaux G, *et al.* High-pressure freezing provides insights into Weibel-Palade body biogenesis. J Cell Sci, 2007; 120: 2117-2125.
[37] Neumuller J, Neumuller-Guber S E, Lipovac M, *et al.* Immunological and ultrastructural characterization of endothelial cell cultures differentiated from human cord blood derived endothelial progenitor cells. Histochem Cell Biol, 2006; 126: 649-664.
[38] Raposo G, Marks M S, Cutler D F. Lysosome-related organelles: driving post-Golgi compartments into specialisation. Curr Opin Cell Biol, 2007; 19: 394-401.
[39] Yang J, Yu J, Li D, *et al.* Store-operated calcium entry-activated autophagy protects EPC proliferation *via* the CAMKK2-MTOR pathway in ox-LDL exposure. Autophagy, 2017; 13: 82-98.
[40] Matsushita M, Suzuki N N, Obara K, *et al.* Structure of Atg5.Atg16, a complex essential for autophagy. J Biol Chem, 2007; 282: 6763-6772.
[41] Hung H S, Yang Y C, Lin Y C, *et al.* Regulation of human endothelial progenitor cell maturation by polyurethane nanocomposites. Biomaterials, 2014; 35: 6810-6821.
[42] Simon H U, Friis R, Tait S W, *et al.* Retrograde signaling from autophagy modulates stress responses. Sci Signal, 2017; 10.
[43] Liu X, Rothe K, Yen R, *et al.* A novel AHI-1-BCR-ABL-DNM2 complex regulates leukemic properties of primitive CML cells through enhanced cellular endocytosis and ROS-mediated autophagy. Leukemia, 2017; 31: 2376-2387.
[44] Settembre C, Di Malta C, Polito V A, *et al.* TFEB links autophagy to lysosomal biogenesis. Science, 2011; 332: 1429-1433.
[45] Brunk U T, Terman A. Lipofuscin: mechanisms of age-related accumulation and influence on cell function. Free Radic Biol Med, 2002; 33: 611-619.
[46] Mizunoe Y, Sudo Y, Okita N, *et al.* Involvement of lysosomal dysfunction in autophagosome accumulation and early pathologies in adipose tissue of obese mice, Autophagy, 2017; 13: 642-653.
[47] Zhang D, Chang S, Jing B, *et al.* Reactive oxygen species are essential for vasoconstriction upon cold exposure. Oxid Med Cell Longev. 2021; 2021: 8578452.
[48] Ruperez C, Blasco-Roset A, Kular D, *et al.* Autophagy is involved in cardiac remodeling in response to environmental temperature change. Front Physiol, 2022; 13: 864427.
[49] Sun H J, Nie X W, Yu K Y, *et al.* Therapeutic potential of gasotransmitters for cold stress-related cardiovascular disease. Frigid Zone Medicine, 2022; 2(1): 10-24.
[50] Fan J F, Xiao Y C, Feng Y F, *et al.* A systematic review and meta-analysis of cold exposure and cardiovascular disease outcomes. Front Cardiovasc Med, 2023; 10: 1084611.
[51] Francula-Zaninovic S, Nola I A. Management of measurable variable cardiovascular disease' risk factors. Curr Cardiol Rev, 2018; 14(3): 153-163.
[52] Chen J, Xavier S, Moskowitz-Kassai E, *et al.* Cathepsin cleavage of sirtuin 1 in endothelial progenitor cells mediates stress-induced premature senescence. Am J Pathol, 2012; 180: 973-983.